Food Research International 155 (2022) 111102

Contents lists available at ScienceDirect

Food Research International

journal homepage: www.elsevier.com/locate/foodres

Review

Hyperspectral imaging for the classification of individual cereal kernels according to fungal and mycotoxins contamination: A review

Antoni Femenias [a], Ferran Gatius [b], Antonio J. Ramos [a], Irene Teixido-Orries [a], Sonia Marín [a,*]

[a] Applied Mycology Unit, Food Technology Department, University of Lleida, AGROTECNIO-CERCA center, Av. Rovira Roure 191, 25198 Lleida, Spain
[b] Department of Chemistry, University of Lleida (UdL), Av. Rovira Roure, 191, Lleida 25198, Spain

ARTICLE INFO

Keywords:
Cereal sorting
Mycotoxins
Fungal infection
Hyperspectral imaging
Single-kernel analysis

ABSTRACT

One of the most common concerns in the cereal industry is the presence of fungi and their associated mycotoxins. Hyperspectral Imaging (HSI) has been proposed recently as one of the most potent tools to manage fungal associated contamination. The introduction of a spatial dimension to the spectral analysis allows the selection of the specific regions of the sample for further screening. Single kernel analysis would enable the discrimination of the highly contaminated kernels to establish a mitigation strategy, overcoming the contamination heterogeneity of cereal batches. This document is a detailed review of the HSI recently published studies that aimed to discriminate fungi and mycotoxin contaminated single cereal kernels. The most relevant findings showed that fungal infection and mycotoxins levels discrimination accuracies were above 90% and 80%, respectively. The results indicate that NIR-HSI is suitable for the detection of fungal-related contamination in single kernels and it has potential to be applied at food industry stages.

1. Introduction

Cereal quality and safety are common concerns for farmers and the food industry. Thus, different approaches have been proposed to assess quality parameters and contaminants. One of the most engaging strategies regarding this aim would be to identify and remove non-desired or highly-contaminated cereal kernels from batches before industry entrance, working as a sorting-based technique. Hyperspectral imaging (HSI) has been considered suitable for contaminated single kernels identification and discrimination during cereal processing steps. Besides, HSI calibration can focus on different physical appearances and chemical substances identification. Thus, HSI can simultaneously perform multiple rapid and non-destructive analyses once validated (Boldrini, Kessler, Rebnera, & Kessler, 2012; Manley, 2014). HSI presents several advantages beyond other conventional methods of chemical analysis. Imaging-based systems are fast in analysing samples compared to chromatographic and immunologic methods. Hyperspectral imaging devices commonly acquire a full image at a timescale of 10 s to 1 min, although it depends on the size of the scanning area and the spectral resolution (Jarvis et al., 2017). Although chromatographic high sensitivity and specificity, HSI is cost-effective and non-destructive for routine analysis in cereal-based industries. In addition, the interest in green analysis methods is increasing to develop new approaches in chemical analysis. HSI uses light sources to detect sample features, substituting pollutant reagents with eco-friendly sources (Caporaso, Whitworth, & Fisk, 2018).

Cereal sorting after reception would be interesting to remove only the kernels that do not accomplish the established quality and safety parameters. Laboratory scale HSI systems have been proposed as a suitable technique to detect individual grains quality and safety parameters (e.g. protein, starch, moisture, hardness, fungal contamination, mycotoxins, defects, etc.) (Fox & Manley, 2014). Several studies used robust statistical models to manage these parameters and to accomplish the established quality and safety standards. Fungi can be present in some kernels of a batch while the rest remain uncontaminated, caused by the heterogeneous contamination of ears or spikes in the field (Lu, Saeys, Kim, Peng, & Lu, 2020). For that reason, a minority of the kernels present high contaminations, which can be responsible for a whole batch rejection in the industry based on sampling and analysis steps (Shahin & Symons, 2012).

2. Principles of the hyperspectral imaging

HSI is an emerging technology that works with the combination of the spectral and spatial information of the samples. The image captured

* Corresponding author at: Food Technology Department, University of Lleida, Av. Rovira Roure 191, 25198 Lleida, Spain.
E-mail address: sonia.marin@udl.cat (S. Marín).

https://doi.org/10.1016/j.foodres.2022.111102
Received 20 January 2022; Received in revised form 3 March 2022; Accepted 4 March 2022
Available online 8 March 2022

Nomenclature

HSI	Hyperspectral imaging
ROI	Region of Interest
Vis	Visible
NIR	Near Infrared
SK-HSI	Single Kernel Hyperspectral Imaging
CCD	Charge-Coupled Device
PCA	Principal Component Analysis
LC-MS	Liquid Chromatography – Mass spectrometry
HPLC	High Performance Liquid Chromatography
GC–MS	Gas chromatography – Mass spectrometry
ELISA	Enzyme-Linked Immunosorbent Assay
ELM	Extreme Learning Machine
JSRC	Join Sparse Representation-based Classification
ANN	Artificial Neural Networks
K-NN	K-Nearest Neighbors
FDK	*Fusarium* damaged kernels
FI	*Fusarium* index
FHB	Fusarium Head Blight
RF	Random Frog
DON	Deoxynivalenol
CM	Confusion Matrix
OTA	Ochratoxin A
ISSPA	Iterative Selection of Successive Projections Algorithm
PW	Pixel Wise

contains spectral information at a specific wavelength range for each pixel. Thus, it bases on three axes: two spatial axes (X, Y) and a third spectral axis (λ), which results in tridimensional information called a hypercube. The desired regions of the samples are selected from the data cube. Then, the spectra corresponding to those regions are extracted and used for further chemometric calibrations (Jiang, Zhu, & Tao, 2010). Fig. 1 shows a representation of the hyperspectral imaging basis. The spectral regions obtained depend on the device used (visible, near-infrared, mid-infrared, etc.). However, the most commonly used are the Visible (400–700 nm) and Near Infrared (700–2500 nm). The Vis region is more frequent in physical features detection, such as defects, colour changes, and damages, while the NIR and SWIR regions are more common for chemical compounds and water content. However, both Vis and NIR regions have combined to enhance the information acquisition of the samples (Walsh, Blasco, Zude-Sasse, & Sun, 2020). The technological readiness of Vis/NIR cameras compared to other spectral regions like the mid-IR allows for fast image acquisition proving the potential of the technology for online implementation in industrial stages. Despite NIR commonly acquire faster measurements than MIR, the time-dependence of the imaging methods is subjected to the measurement mode (e.g. snapshot is faster than push-broom mode), the number of scans and the spectral resolution. Thus, online HSI analysis requires balanced settings between analysis speed and the acquisition of sufficient spectral information to detect the target compound.

2.1. HSI equipment

HSI components include an optical system, spectrometer, illumination unit, computer, and moving unit. The optical system registers the spectral and spatial information of the sample by three components (Bellon-Maurel & Gorretta, 2014). The first component is the HSI camera is usually a charge-coupled device (CCD) camera that includes semiconductor electronic properties (Kim & Chen, 1998). The second optical component is the spectrometer, whose function is the dispersion of the light in different wavelengths to obtain the spectrum of each pixel in the image. Finally, the objective lens function focuses the light from the illuminated object through the spectrometer and the HSI camera detector. The illumination unit should produce homogeneous light to

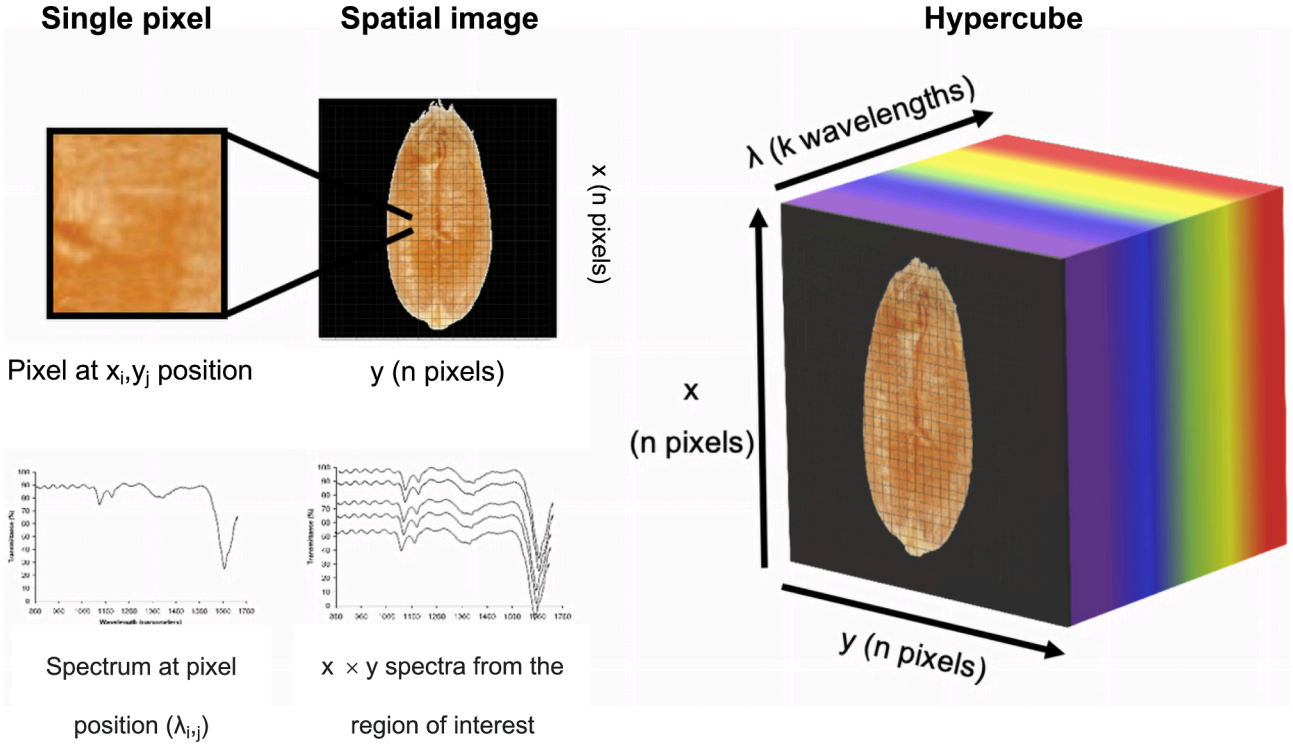

Fig. 1. Basis of the hypercube in hyperspectral imaging. Relationship between the spatial resolution (x, y) and the spectral resolution (λ).

avoid any alterations in sample radiation. Thus, the illumination unit lights the scanned object while the camera moves above it, or the object moves under the camera field of vision under controlled conditions. A typical laboratory-scale moving system consists of two parts, the translation stage, which is the support of the sample, and the motor, which controls the speed of the movement for correct image acquisition. Both imaging and moving systems are attached to a computer equipped with control software (Mahesh, Jayas, Paliwal, & White, 2015). In addition, some field screening studies use aerial imaging, where the camera is moving on the target surface, and the area of study remains fixed. It is applied to detect population changes, geological transformations and archaeological sites. Moreover, the HSI software set all the scanning parameters, like the scanning speed, the framerate, and the integration time are selected (Yao & Lewis, 2010). Fig. 2 represents a conventional hyperspectral imaging system.

3. Common single kernel analysis process

The single kernel hyperspectral imaging (SK-HSI) permits the spatial selection within the sample. Thus, the Region of Interest (ROI) goes far beyond the whole measured object and can consist of a single kernel screening or single sections within the kernel, like bran, germ, midsection, endosperm, pericarp, etc. The captured image contains the spectral information of the n × n pixels from the kernel/part, removing the background manually or automatically. Some authors focused on SK-HSI analysis (Fox & Manley, 2014). The main advantage of this analysis is to overcome the heterogeneity of cereal samples. Thus, the methodology used for HSI calibrations also requires the characterization of the single kernel features to distinguish their characteristics within a batch. Fig. 3 represents a typical SK-HSI analysis flowchart.

3.1. HSI scanning modes for single kernel analysis

The HSI devices present different image scanning modes. The most commonly used are the push-broom, whisk-broom, staring imaging, and snapshot. The push-broom measurement (line-scanning) mode consists of the spectral data acquisition by pixel lines. The measured object moves in the y-axis direction, while the imager is recording the spectrum of the pixels in the x-axis direction. This mode presents good spatial and spectral resolutions. For that reason, it is the most widely used in HSI calibrations for online and inline scanning because the objects are moving under the field of view, making possible real-time analysis and sorting operations (e.g. depositing the cereals on a conveyor moving under an HSI system) (Qin et al., 2017). The whiskbroom method (point-scanning) involves the successive acquisition of the spectral information of single pixels by moving the sample or the sensor. As the camera and the detector are moving while scanning, the device requires imaging pathways to record the 2D field of vision from the sample. The staring imaging (band-scanning) ensures a full 2D-area recognition, obtaining only the spectral information of a single band. Instead of dispersing the light in multiple wavelengths in front of the detector, it commonly uses a bandpass filter after the light has passed through the objective lens. Thus, a narrowband segment is produced and perceived by the sensor. Finally, snapshot imaging (single-shot) limits exposure time by a single shot to scan both spectral and spatial information (Qin, 2010). Thus, the sample is not moving under the scanning region, as a complete image is acquired instantaneously, while the CCD camera records the entire image spectral information. The main advantage of snapshot mode is the minimum scanning time that it does not require post-processing for the 3-D hypercube formation. Nevertheless, it presents a limited spectral and spatial resolution as the number of voxels scanned cannot exceed the maximum accepted by the CCD camera. Consequently, it only records the sample fixed region (ElMasry & Sun, 2010).

3.2. ROI extraction

In SK-HSI analysis, the pixel intensities from the kernel are considered the ROI. The ROI is a defined image area selected for further processing and analysis. Single or multiple image regions can be used for subsequent analysis. HSI images do not contain only a high amount of chemical data but also textural, morphological, and intensity characteristics (Sahu, 2014). In addition, as the contamination is heterogeneous within a single kernel, HSI can overcome the differences within grain by extracting a single or region of pixels selection (bran, endosperm, germ, pericarp, or other desired parts). The characterization of smaller areas in the grain can decrease light non-uniformities and

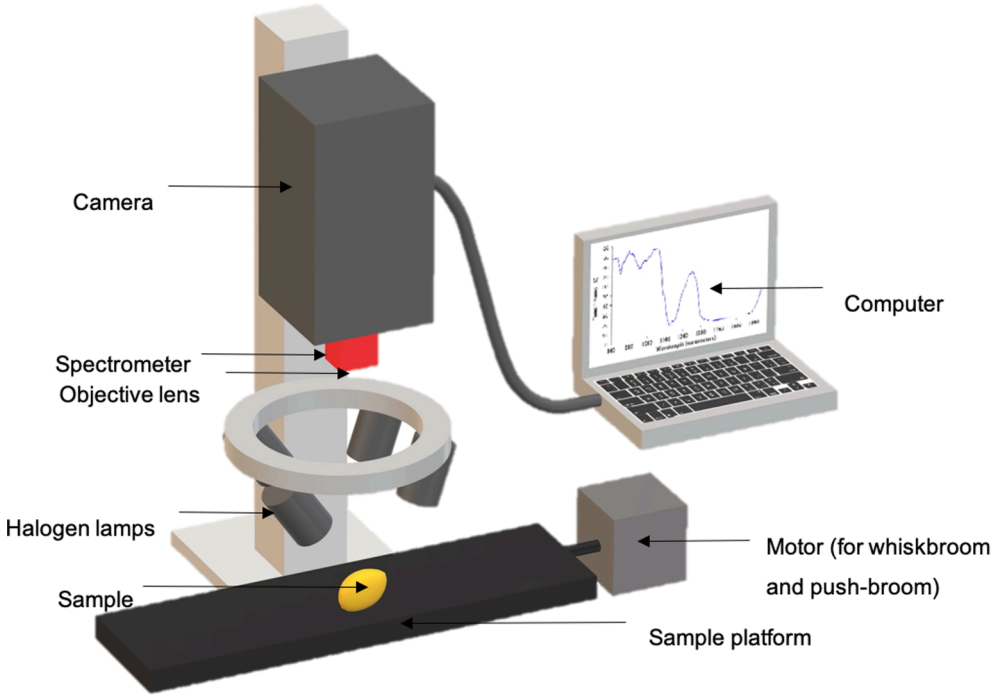

Fig. 2. HSI acquisition system.

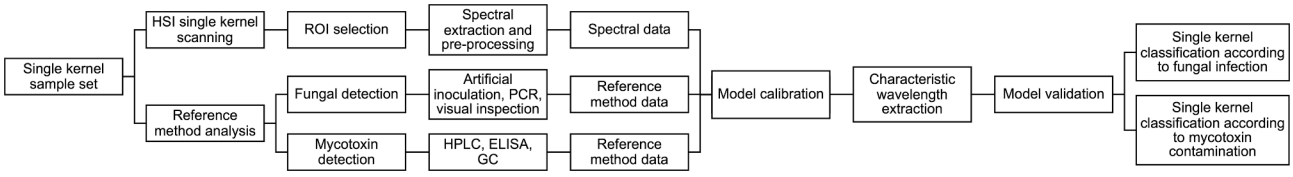

Fig. 3. Flowchart of the most common SK-HSI analysis process of cereals for fungal and mycotoxin contamination.

shadowing, as, because of the kernel shape, light interacts differently along with their parts. For images with higher contrast between the sample and the background, it is easier to remove background from the ROI, and, thus, the thresholding procedure also becomes more accurate. There exist different ways to extract the ROI from a single kernel or specific parts of the grain. The most frequently used are spectral mask image segmentation, manual selection and exploratory principal component analysis (PCA). The spectral mask application was used in some studies by the segmentation of the background using a single spectral band image, which consists in the background removal using the band with higher contrast between the ROI and the redundant parts of the image (Barbedo, Guarienti, & Tibola, 2018; Barbedo, Tibola, & Fernandes, 2015; Lu et al., 2018). Manual selection is the less complex approach for ROI selection. The desired part of the image can be extracted by the manual delimitation ROI or by the selection of groups of pixels with similar intensities to the target pixels (Femenias, Bainotti, Gatius, Ramos, & Marín, 2020; Zhang, Li, Takeda, & Yang, 2017). Euclidean distance or spectral angle selection is also frequent. Despite the simplicity of these ROI delimitation methods, they are less automated, requiring user selection and longer procedure times. Chemometric tools have been applied to remove the irrelevant pixels from the image. PCA has been used to select the ROI from the non-processed images by dividing pixels intensities into two groups according to the projection in a score plot. Pixels that correspond to the background were brushed, obtaining a new image that contains only the pixels from the ROI (Williams, Geladi, Britz, & Manley, 2012; Williams, Manley, Fox, & Geladi, 2010).

3.3. Measurement modes

The most commonly used and well-known measurement modes are diffuse reflectance, transmittance, interactance, and transflectance. The interaction between the light beam and the sample can be recorded in different ways. Some measurement modes are more suitable for specific samples depending on the nature of its matrix, as the light has different behaviours depending on the chemical and physical properties (Pasquini, 2003). The differences produced in light reflection due to its interaction with the cereal sample have to be correctly recorded and interpreted to correlate them with changes in chemical composition or physical features of the sample.

In diffuse reflectance mode, the emitted beam from the light source reflects on the sample surface and partially penetrates in the sample with multiple different angles. Thus, the light diffusion and penetration in the sample change depending on the chemical and physical properties, detecting their structural and compositional parameters. When the sample works as a mirror, specular reflectance occurs. The light beam reflects at the same incident angle, overlapping the physical and chemical information. Consequently, the brightness differences are not detected (Lu, Huang, & Lu, 2017). In transmittance mode, the light ray passes through the sample to the opposite side from the light source, where the detector records the intensity. This sensing mode is ideal for liquid and homogenized samples, and it offers reduced information for solid opaque samples. Therefore, it is not an appropriate measurement mode for cereal evaluation. Apart from the reflectance and transmittance modes, the interactance is available, for which the illumination beam penetrates deeply into the sample, as the detector is situated far from the light ray. The main mode advantage is that it does not obtain only the sample surface information but also the inner part characteristics. However, it is problematic for high translation scanning speeds because it needs longer capture times (Schaare & Fraser, 2000). Finally, the transflectance mode consists of a duplicated light passing through the sample by light intensification with a mirror located at the opposite side of the illumination unit. This mode is frequent in pasta studies.

3.3.1. Calibration of the measurement modes

The HSI devices present by default the reflectance, transmittance, interactance or transflectance measurements in absolute values. Thus, before the HSI scanning, the calibration of the equipment is required to register relative values concerning the maximum and minimum signals. The calibration principle is common for the different measurement modes (reflectance, transmittance, etc.). In all the cases, the relative values are obtained by correcting the dark and white reference from the image. In the reflectance mode, the image is corrected by considering the white reference as the image of a fluoropolymer of the maximum known reflectance (99 %) and the dark reference as the image taken with the lens covered and the lights turned off (0%). The calibration of transmittance HSI devices differs slightly from the abovementioned procedure, obtaining the 100 % transmittance image using a glass table (Kandpal et al., 2020). Equation (1) presents the mathematical expression of the dark and white reference images correction.

$$X_C = \frac{I^R_{x,y}(\lambda) - I^b_{x,y}(\lambda)}{I^w_{x,y}(\lambda) - I^b_{x,y}(\lambda)} \quad (1)$$

where X_C is the corrected image; $I^R_{x,y}(\lambda)$ is the raw hyperspectral image obtained; $I^w_{x,y}(\lambda)$ is the white reference; and $I^b_{x,y}(\lambda)$ is the dark current reference.

3.4. Reference method of analysis

HSI, as other spectroscopic technologies, requires a calibration for the analytical purpose. The calibration of supervised models, such as prediction or classification, are supported by a reference method, which introduces de independent variables to the algorithm. The model performances directly depend on the sensibility of the reference method, thus a reference method with low deviations and high sensitivity is desired to support the model. The reference method for quantitative prediction of chemicals is usually the concentrations of the training sample set, while for classification the samples are categorized into qualitative features used to supervise the classification models.

For quantitative prediction of fungal contamination, molecular-based techniques, such as PCR, have been used in cereal kernels. PCR as reference method allows for fungal identification and quantification Polder, van der Heijden, Waalwijk, & Young (2005) used PCR as reference method to identify *Fusarium culmorum* with concentrations above 6000 pg on maize kernels by NIR-HSI. Instead of obtaining DNA from cereals, Da Conceição et al. (2021) extracted DNA from fungal isolates for molecular analysis to identify *F. graminearum* and *F. verticillioides* with an accuracy of 100%. On the other hand, Alisaac et al. (2019) analysed wheat flour by quantitative PCR and correlated the values with Vis/NIR-HSI.

Alternatively, the artificial inoculation ensures the fungal presence in the grains at controlled conditions (strains, amount, growth stage, etc). Unlike naturally contaminated samples (the contamination has to

be spontaneous in the field), fungal inoculation ensures mycotoxins presence in samples with controlled fungal amounts (Karuppiah, Senthilkumar, Jayas, & White, 2016; Tekle, Mage, Segtnan, & Bjornstad, 2015). Model calibrations should adjust to the contaminations commonly found in the field and postharvest stages. Consequently, the use of artificially inoculated sample sets with extremely-high fungal amounts usually presents high mycotoxins contaminations, not found commonly in the field. Such studies using high values of mycotoxins are valuable for laboratory-scale purposes, although their contamination levels are higher than the found in previous stages to cereal industry entrance.

The most frequently used method is visual inspection. It consists of the kernels feature observation and characterization by a trained expert. Features visual determination is fast, non-destructive and non-pollutant. Nevertheless, it presents some disadvantages, as the subjectivity of the employee, low sensitivity, and it only allows qualitative determinations. Numerous studies used visual inspection as the reference method for SK-HSI calibration (Delwiche & Kim, 2000; Delwiche, Kim, & Dong, 2010, 2011; Delwiche, Rodriguez, Rausch, & Graybosch, 2019; Ropelewska & Zapotoczny, 2018; Shahin & Symons, 2012).

Finally, quantifying some predominant chemical compounds in fungal cell structure can determine the levels of fungal infection. Ergosterol is a chemical compound found in the fungal cell wall, and it is absent or minority in plant structures. Thus, it is a target substance for fungal contamination assessment. As ergosterol is a specific compound found in all fungi, it does not offer information on any genus. Thus, the calibration of this compound would give a general fungal contamination evaluation in cereal products (Femenias, Gatius, Ramos, Sanchis, & Marín, 2021).

The most frequent reference methods used to calibrate HSI for mycotoxin detection are LC-MS, HPLC-DAD, GC–MS, and ELISA. These methods present high sensitivity and specificity, providing low deviations to the calibration models. In addition, there exist official methods of analysis of mycotoxins in cereals, which ensure the correct quantification of these compounds. However, those methods used in wet chemistry analysis present a limited sample representation, as from a batch of several tones, only several grams are analysed in the laboratory according to the official control of analysis of mycotoxins in foodstuffs (European Commission, 2006b), being an issue in heterogeneous batches analysis. In addition, the use of green analytical approaches is increasing to avoid environmental pollution caused by the mentioned routine reference methods used. Nevertheless, some authors used different methodologies from the official ones to determine the mycotoxin levels in single kernels (Femenias, Bainotti, et al., 2021; Liang et al., 2020; Tekle et al., 2015).

3.5. Modelling techniques

Hyperspectral data are composed of a massive amount of data that require the extraction of conclusions about the analysed material. Preprocessing techniques allow data reduction for easier handling. However, after this step, a large variables number remains, requiring chemometric tools to build classification approaches. Several modelling methods exist for grouping, pattern recognition, feature discrimination, etc. The most well-known are principal component analysis (PCA)-based techniques; discriminant analysis, such as linear, quadratic and Mahalanobis, or partial least squares discriminant analysis (PLS-DA); and support vector machines (SVM). Nevertheless, there are numerous credible alternatives to the abovementioned methods for kernels grouping according to one or more features, reviewed in the following sections.

PCA can reduce high-dimension data to fewer components in a new subspace of vectors, containing the most valuable part of the information. The main action of PCA is to project data to select the relevant data and discard the non-useful information. This tool assumes that the relevant information corresponds to the variables with higher variance. PCA has projection ability and exploratory data analysis, even it cannot be used as a classifier. Thus, PCA extensions are applied, such as factor analysis (FA), discriminant analysis (DA), cluster analysis (CA), etc. The studies demonstrated that PCA transformation into a dimensionally-reduced subset of vectors in combination with extension classifiers improves the precision of the models (Novakovic & Rankov, 2011).

One of the most widely used methods for classification purposes in HSI studies is the DA, which is based on features recognition to separate the observations into different groups. Several DA approaches are available, such as linear, quadratic and Mahalanobis. Linear discriminant analysis (LDA) assumes shared covariance between the two or more classification groups. LDA can divide into classes by linear combination, which maximizes the ratio between the variances of the observations and the corresponding group. Nevertheless, LDA collinearity presents problems to predict the dependent variable values independently. Quadratic discriminant analysis (QDA) is an alternative to LDA, for which the covariance is individual for each group of observations. Thus, in QDA, it should be known in advance if the classes have different covariances, as it uses a covariance matrix for each group. In addition, this technique does not permit a data dimensionality reduction. Some studies used Mahalanobis based LDA, considering the differences in the dispersion and the orientation. It follows a different procedure from the conventional LDA, for which first the Mahalanobis distance from the populations is calculated to classify the closer element and then the groups are compared two by two (Ito, Srinivasan, & Izumi, 2006).

To avoid the previously-mentioned problems of the DA, the partial least squares discriminant analysis (PLS-DA) is an algorithm combination of DA and dimensionality reduction for the application in high data volumes. This technique has been applied in different fields of science because it is not as strict as LDA in data fitting (LDA cannot adjust data with distribution). Consequently, PLS-DA has been applied to numerous studies with classification and grouping purposes (Lee, Liong, & Jemain, 2018). Lastly, another classification approach extensively used in classification is Support Vector Machines (SVM). The basic principle of SVM is the construction of a hyperplane that can correctly divide a broader percentage of observations into classes. The hyperplane consists of a vector between two points of the two groups. Thus, the SVM presents advantages in kernel classification as the maximum robustness of the high-dimension of HSI data and low sensitivity to the number of observations (Jiang et al., 2010).

Numerous alternatives to the abovementioned statistical classifiers are available with the aim of kernel classification by HSI, such as sparse autoencoder (SAE), self-organizing map (SOM), extreme learning machine (ELM), joint sparse representation-based classification (JSRC), artificial neural networks (ANN), k-nearest neighbours (KNN), SAM classifier, confusion matrix, binary encoding, random forest, maximum likelihood, etc.

4. Applications of HSI on single kernel classification according to fungi and mycotoxins

Fungi and their associated mycotoxins produce a negative economic impact on cereal production. Batch rejections before industry entrance are the main causes of yield reduction of cereal producers. Thus, new post-harvest strategies to reduce fungal and mycotoxin contamination are required. HSI classification has been proposed to differentiate between infected and healthy kernels. This technique would allow the identification and removal of highly-contaminated grains from cereal batches to reduce the overall contamination. Recently published studies to classify grains according to these contaminants are exposed and discussed in the following sections.

4.1. Optical changes produced by fungal growth

Fungal metabolism produces physical and chemical changes in cereals. Physical changes in single kernels are detected, such as structural

changes (kernel size, kernel shape and shrivelling) and colour changes (discolouration and pinkish). On the other hand, noticeable chemical changes produced by fungi are inherent to their growth, as changes in protein, starch, lipid and water composition. Inherent spectral changes are produced due to the differences in matrix composition. Thus, the optical changes are useful to monitor fungal growth and associate mycotoxins production in cereal products. In addition, long-wavelength regions are more appropriate to measure the low concentration matrix components, as they require shorter optical path length and penetration depth.

Structural changes and chemical decompositions affect different spectral regions on the NIR window. Kernel size differences produce baseline offset, as the thicker kernels will have a deeper penetration of the light, and the absorbance will be higher (Chu, Wang, Ni, Li, & Li, 2020). Otherwise, the cereal kernels brightness, caused by kernel infections, changes in the late visible spectral region (628–706 nm) (Su et al., 2021). Dowell, Ram, & Seitz (1999) correlated the differences caused by fungal infection in protein and starch content with 1400 nm region for its use as indirect detection of DON in cereals. Nevertheless, Peiris, Pumphrey, & Dowell (2009) studied NIR absorption for fungal damage and DON. In the first instance, they identified the NIR changes produced by shrink and brightness in FDK, two well-known differences produced by a fungal infection. Spectral differences were in the 1425–1450 nm region, where FDK kernels showed a shifted peak at 1445 nm, while sound kernels were in 1430 nm. Liang et al. (2020) attributed the changes produced around 1190–1212 nm (2nd overtone of C–H stretching vibration) to variations of some principal storage compounds, such as starch and fat content. In addition, the region between 1733 and 1778 nm (1st overtone C–H) is related to amylose, a majority component of the starch. The authors also attributed higher radiations (1935–1952 nm) to the combinations of stretching and bending of water molecules. Finally, protein changes in NIR spectra were in the 1446–1502 nm, corresponding to the 1st overtone of N–H. Otherwise, N–H stretching related to CONH2 in maize proteins was related to absorbance deviations in the 1520 nm region by Chu et al. (2020). In addition, they detected variations in functional groups of oils and fatty acids due to fungal infection in the 1666–1818 region. Phenolic content produced by vegetal products also experienced a difference between damaged and healthy kernels, presenting intensities alterations in 1415–1512 nm.

NIR spectral differences detection produced by DON is complex for its low concentrations. However, Peiris et al. (2009) identified the spectral characteristics for pure DON solution in acetonitrile and FDK. The authors recognized two NIR regions (1390–1440 nm and 1880–1950 nm) that differ with DON concentration, analyzing pure DON. Two characteristic peaks near these regions related to DON 1st overtone in 1414 nm for O–H bonds and 1906 nm for -C = O and R–OH. *Fusarium* damage correlated with DON at the NIR region, detecting most alterations at 1204, 1365 and 1700 nm bands, related with 1st overtone alterations in C–H groups in reserve compounds of grains (carbohydrate, lipids and proteins).

Almost all the studies reviewed attempted the optimal latent variable (LV) selection. The number of wavelengths selected is variable, and it goes from 1 to 20 LV, using different selection strategies. Even though the LV selection does not improve model performance in all the studies, it offers a reduction in data dimension is interesting from the point of view of computational time in online sorting strategies, which remove the contaminated kernels in situ. The characterization of the selected wavelengths is also fundamental for the changes produced by fungi on cereals in correlation with the spectral profile obtained. Optimal selection is crucial in the technique application for sorting purposes. Consequently, Although the present results demonstrated accurate wavelength selections, work advances on this item is required in future studies.

4.2. SK-HSI classification according to fungal contamination

Fungal contamination is responsible for the quality and production of cereal crops reduction. Fungal growth produces several changes on cereal kernels structure that can be visualized as weight loss, shrivelling, discolouration, etc. Several authors propose the visible (400–700 nm) and the near-infrared (780–2500 nm) regions of the electromagnetic spectrum for fungal detection in single cereal kernels. Therefore, classification models are proposed for cereal sorting according to fungal species or the symptomatology caused on the grain. The classification accuracies estimate the model performance, which gives the correctly classified percentage of the kernels.

In this section, the studies focused on single kernels as the ROI for fungal infection assessment are reviewed and compiled in Table 1. In recent years, several studies on single wheat kernels have been published. The two most studied fungal genera in kernel sorting publications are *Aspergillus* and *Fusarium* for their associated impact on grain quality and associated negative health effects. Zhang, Paliwal, Jayas, & White, (2007) and Singh, Jayas, Paliwal, & White (2012) discriminated between non-contaminated kernels and fungal-infected kernels by *Penicillium spp.*, *Aspergillus niger*, and *A. glaucus* in the NIR region. Before HSI analysis, the kernels were artificially contaminated with fungal spores and incubated to let them grow. The artificial inoculation ensures fungal growth but, depending on the inoculation, it can present different contamination levels than the natural inoculation, which presents levels commonly found in the field. Artificial fungal inoculation offers some advantages, such as controlled growing conditions and selected strains. However, the changes produced on cereals differ from the naturally infected, which experience contamination with more than one fungal strain and at variable contamination levels. Consequently, we consider artificial inoculation a suitable approach for laboratory-controlled preliminary studies, despite further investigations on independent and naturally-infected kernels should be performed. Although they used different chemometric tools to calibrate the models, both studies obtained positive results above 87% of correctly classified kernels. Other studies classified wheat kernels as healthy or infected with *Fusarium* species, such as *Fusarium graminearum*, *F. culmorum*, and *F. poae* in the visible and NIR region. Ropelewska & Zapotoczny (2018) used visual inspection as the reference method, unlike Alisaac et al. (2019), which used qPCR in their study. Ropelewska & Zapotoczny (2018) used Bayes, LDA, K-Star, Rules PART and Decision Tree classifiers, obtaining accuracies between 78 and 100%. On the other hand, Alisaac et al. (2019) represented their results as differences in the spectral signature of the scanned kernels instead of evaluating the percentage of correct classification. This study used the differences in several spectral regions to correlate them with fungal presence and DON. Despite the obtained good correlations, spectral characterization in the NIR region is complex due to the peak overlapping, especially in high-frequency regions (low wavelengths). The spectral resolution is increased in far NIR regions of Mid Infrared (MIR), in which spectral peaks regarding chemical substances on cereal composition can be suitably identified (Kos et al., 2016). Thus, the study discussed that chemometric tools could model the spectral data to extract deeper information and avoid overlapped information. However, the spectral signature correlation with contamination features indicated good-quality raw data. The alternative to artificial fungal inoculation is the visual changes produced during natural fungal growth assessment. Visual inspection is frequent in studies to determine the damage caused by *Fusarium* infection, which categorizes the kernels as *Fusarium* damaged kernels (FDK) according to their weight loss, shrivelling and discolouration. Despite the simplicity of this method, it is less reliable than chemical or biological techniques due to the subjectivity of the inspector. Several authors used LDA as a classification tool for FDK (Delwiche et al., 2019; Femenias, Bainotti, et al., 2021; Shahin & Symons, 2011). They presented highly accurate results between 92 and 100% of correctly classified kernels. Despite the high accuracies obtained, the visual inspection categorized kernel damage.

Table 1
Single-kernel hyperspectral imaging studies for the classification of fungal infection in cereals.

Cereal	Fungi	Spectral range N° of LV used	Preprocessing technique	Reference method	Training/test set Total kernels	Classification model and accuracy (%)	References
Wheat	*Aspergillus niger, A. glaucus Penicillium* spp. *(Inoculated)*	900-1700 nm 20 LV	Normalization PCA transformation	Artificial inoculation	400/140 kernels for each mould specie 2160 total kernels	SVM (>87.2%)	(Zhang et al., 2007)
	FDK *(Natural contamination)*	400–1000 nm 6 LV	Normalization Extremes removal	Visual inspection	400/400 (200 healthy and 200 FDK) 800 total kernels	LDA (92%)	(Shahin & Symons, 2011)
	FDK *(Natural contamination)*	1000–1700 nm 4 LV	GLS Weighting	Visual inspection	40/30 70 total kernels (Cross-validated)	PLS-DA (94.4–99.2%)	(Serranti et al., 2012)
	Penicillium spp. *Aspergillus glaucus A. niger (Inoculated)*	700–1100 nm 13 LV	–	Artificial inoculation	240/60 300 total kernels (Independent)	LDA, QDA, Mahalanobis (94–98.3%)	(Singh et al., 2012)
	FDK *(Inoculated)*	528-1785 nm 1 LV	Normalization	Visual inspection	50–100/700–750 803 total kernels	*Fusarium* index (91%)	(Barbedo et al., 2015)
	Fusarium graminearum (Natural contamination)	600–1100 nm 3 LV	–	Visual inspection	120 total kernels (Cross-validated)	LDA, K Star, PART, LMT (78–100%)	(Ropelewska & Zapotoczny, 2018)
	FDK *(Natural contamination)*	938–1654 nm 2–7 LV	Mean centering SNV	Visual inspection	556/20820 21,376 total kernels	LDA, PLS-DA (>92%)	(Delwiche et al., 2019)
	Fusarium culmorum F. poae (Inoculated)	400–2500 nm (Whole range)	–	qPCR	No calibrations performed	Spectral signature (−)	(Alisaac et al., 2019)
	FDK *(Natural contamination)*	900–1700 nm (Whole range)	1st Derivative SNV	Visual inspection	50 total kernels (Cross-validated)	LDA (100 %)	(Femenias, Bainotti, et al., 2021)
Maize	*Aspergillus flavus A. parasiticus A. niger (Inoculated)*	400–1000 nm 3 WL	–	Artificial inoculation	No validation performed	PCA-DA (−)	(Del Fiore et al., 2010)
	Aspergillus flavus (Inoculated)	400-700 nm 2 LV	–	Artificial inoculation	243/249 247/245 492 total kernels	Maximum likelihood: >80% Binary encoding: >87%	(Yao et al., 2013)
	Aspergillus A. flavus A. niger ochraceus (Natural contamination)	900–1700 nm 8–10 LV	–	Fungal isolation	595/297 892 total kernels	PW-PCA-SVM (100%)	(Chu et al., 2020)
	Fusarium verticillioides F. graminearum (Inoculated)	1000-2100 nm 4 LV	SNV Mean-centering	Fungal isolation	2/13 isolates 15 total isolates	PCA (−) PLS-DA (88–100%)	(da Conceição et al., 2021)
Rice	*Aspergillus oryzae (Inoculated)*	400–1000 nm 10 LV	–	Artificial inoculation Electron microscopy	119/91 kernels 210 total kernels	SOM (−)	(Siripatrawan & Makino, 2015)
	Villosiclava virens (Inoculated)	874–1734 nm Regions selection	Extremes removal	Artificial inoculation PCR	Different sets 1720 total kernels	PLS-DA (98.4%) SVM (98%) ELM (99.2%)	(Wu et al., 2020)
Barley	*Aspergillus glaucus Penicillium* spp. *(Inoculated)*	400-2500 nm 3 LV	–	Artificial inoculation	240/60 300 total kernels	Linear, Quadratic and Mahalanobis discriminant analysis (>94%)	(Senthilkumar et al., 2016)
Pulses	*Aspergillus flavus Penicillium commune (Inoculated)*	900-1700 nm 3 LV	Median filter Extremes removal	Artificial inoculation	- 1800 total pulses	LDA (98–100%) QDA (96–100%)	(Karuppiah et al., 2016)
Peanuts	Fungal contamination *(Inoculated)*	967–2499 nm 15 LV	Five-point smoothing filter SPA	AFB1 immune-chromatographic test	66/58 124 total kernels	JSRC (96.8–99.2%) SVM (90.5–97.6%)	(Qi, Jiang, Cui, & Yuan, 2019)

ELM = Extreme Learning Machine; JSRC = Joint Sparse Representation based Classification; PW = Pixel-wise; SOM = Self-Organizing Map; SPA = Successive Projection Algorithm; SVM = Support Vector Machines.

Thus, low fungal contaminations, which are not visually detectable, are not included in this category, expecting some deviations. Several methods of fungal identification can replace visual inspection weakness, e.g. automatized kernel categorization, fungal isolation, fungal DNA quantification, among others. Chemometric alternatives to LDA were also used, as PLS-DA, applied in the study of Serranti, Cesare, & Bonifazi (2012) and Delwiche et al. (2019) for wheat kernels sorting according to the damage caused by a fungal infection. The first study obtained

accurate classifications with a percentage of correctness above 94%. Likewise, Delwiche et al. (2019) obtained an overall accurateness of 97.3% and an optimal classification model with four latent variables of 96.8%. Finally, the *Fusarium* index (FI) classified wheat grains according to fungal damage according to the probability of wheat kernels to develop Fusarium head blight (FHB) (Barbedo et al., 2015). The FI based algorithm obtained a classification accuracy of 91%. Generally, the studies aiming at wheat kernels sorting according to fungal infection presented good results. However, the research focused on laboratory conditions and imprecise reference methods. Consequently, field fungal infections and improved reference methods are required to apply the classification models to the food industry.

Although wheat is the most investigated cereal, the fungal infection at the single-kernel level has been assessed in others. Maize is the second most investigated cereal, mainly for *Aspergillus* infection assessment. Del Fiore et al. (2010) and Yao et al. (2013) used similar spectral regions to differentiate previously inoculated *Aspergillus* species, such as *A. flavus*, *A. parasiticus*, and *A. niger*. The first study used PCA to discriminate the species in the Vis-NIR region in different infection stages after artificial inoculation. Yao et al. (2013) focused uniquely on the visible spectra to build two classification models. Alternatively, LDA was performed, obtaining weak results (44.2%). As an alternative, the confusion matrix improved the previous results with a percentage of accuracy of 74.7%. Naturally contaminated kernels with *Aspergillus flavus*, *A. ochraceus*, and *A. niger* were analyzed in the NIR region by Chu et al. (2020). In this study, a complex algorithm composed of pixel-wise, PCA, and SVM was created, obtaining a classification of 100%. Finally, two *Fusarium* species infections (*Fusarium verticillioides* and *F. graminearum*) in maize kernels were analyzed, scanning by HSI after their artificial inoculation (da Conceição et al., 2021). The NIR spectra, preprocessed with SNV and mean-centred, were modelled to calibrate a PLS-DA model with a perfect discriminant accuracy. Maize analysis by HSI should offer advantages compared to cereals with smaller kernel sizes, like wheat and rice. The particle size is directly related to the light penetration in diffuse reflection or transmittance modes. Maize size permits deeper penetration of incident radiation and, thus, provides enhanced information for the inner part of the kernels. In small kernel analysis, the surface information influences the overall data. In addition, the comparison between cereal types is not possible due to different light incidence angles and shadowing effects. Some studies applied HSI for rice analysis. Vis-NIR HSI analyzed artificially inoculated *Aspergillus oryzae*, previous to electronic microscopic examination. An unsupervised SOM visually assessed the different fungal contamination levels (Siripatrawan & Makino, 2015). Alternatively, supervised methods based on PLS-DA, SVM, and ELM detected artificially contaminated *Villosiclava virens* in rice kernels (Wu et al., 2020). They acquired the NIR spectra before analyzing the rice by PCR. Thus, several discrimination models, such as PLS-DA, SVM, and EML, were calibrated, using the data obtained from both methods. Although all the models achieved accuracies above 99.4% in the validation set, the best was the Random Frog (RF)-ELM with correctness of 99.2%. The study of Senthilkumar, Jayas, White, Fields, & Gräfenhan (2016) evaluated barley kernels according to previously inoculated *Aspergillus glaucus* and *Penicillium spp*. in the Vis-NIR region. They used different discriminant analyses (linear, quadratic, and Mahalanobis) for which a classification accuracy of barley kernels was>94%.

Finally, other studies, including food products other than cereals that also evaluate fungal infection in individual kernels, were also reviewed. The example of legumes, which have a similar shape as cereal kernels, could be handled using similar methodologies for HSI analysis. The study of Karuppiah et al. (2016) evaluated the fungal infection in different pulses, including chickpeas, green peas, lentils, pinto beans and kidney beans. They evaluated previously inoculated legumes for QDA and LDA modelling by an NIR-HSI analysis. The results were similar for both models, despite LDA achieving slightly better classifications (98–100%). Finally, fungal contamination in peanuts was also studied, using the algorithms based on JSRC and SVM for individual peanut kernels discrimination. The accuracies derived from 96.8 to 99.2% in JSRC models and 90.5–97.6% depending on the threshold and the peanut variety. The amount of mildew spores on maize kernels was predicted using Raman HSI by Long, Huang, Wang, Fan & Tian (2022), combining textural and spectral information. The amount of mildew spores was divided in 6 levels to calibrate the models. The performance of the optimum model for an independent validation set was R^2 of 0.80 and RMSEP of 0.87. Considering the results, the calibration of classification models would be more suitable for the discrimination of single kernels according to the established spore levels by the reference method than the predictive algorithms.

Taken together, the overall results in SK-HSI reviewed studies are positive, achieving classification accuracies above 90% in most cases. The results are promising for HSI technologies implementation in the food industry aiming at cereal sorting according to fungal infections. Despite the high accuracies, before SK-HSI for routine analysis application, further studies are required, including higher data sets using independent kernels for model validations. In addition, models should use natural contaminations to build robust calibrations able to predict and discriminate typical fungal contamination found in the field. Moreover, further studies with more precise reference methods are required to assess the usefulness of method application in industrial sorting processes.

4.3. SK-HSI classification according to mycotoxins contamination

Fungal infection is frequently associated with mycotoxins production, inherent to fungal secondary metabolism. Mycotoxin contamination of cereals is associated with harmful health effects in humans and animals. Consequently, food safety authorities (European Commission, 2006a) established maximum mycotoxins limits in cereal products. According to their potential health risk, the regulated mycotoxins are aflatoxin B1, ochratoxin A, patulin, deoxynivalenol, zearalenone, and fumonisins. Mycotoxins detection with HSI in cereal products is challenging because they do not produce visual changes in kernels, its low levels (low ppm or ppb) in samples regarding other majority substances in the cereals and their heterogeneous distribution in a batch. Notwithstanding the detection difficulties, several authors applied the HSI potential to discriminate the highly-contaminated kernels in a cereal batch (Table 2). DON contamination in wheat and AFB1 in maize are the most studied for HSI mycotoxin assessment.

Several classification procedures are applied to evaluate DON in wheat. Discrimination with the same threshold (1.25 mg/kg) was performed by Barbedo et al. (2015) and Femenias et al. (2020), although they used different classifiers. Confusion matrix (CM) results from the first study obtained an 81% correctness with ELISA as the reference method. Therefore, the LDA results from Femenias et al. (2020) reached 98.9% accuracy. They used 1st derivate preprocessed spectral data combined with the reference values obtained by HPLC analysis. Otherwise, Alisaac et al. (2019) and Liang et al. (2020) used both visible and NIR regions (400–2500 nm) for the non-destructive assessment of wheat kernels. Alisaac et al. (2019) did not use chemometric tools for DON detection. Instead, the significant differences between the spectra according to the mycotoxin concentrations were evaluated, obtaining a correlation of 0.8. Far from the simplicity of spectral signatures, Liang et al. (2020) used a complex computational model based on the combination of MSC, GA and SAE, which separated contaminated kernels above and below 1 mg/kg of DON with an accuracy of 100%. Finally, the study of Senthilkumar, Jayas, White, Fields, & Gräfenhan (2017) studied Ochratoxin A (OTA) contamination in wheat kernels for five different thresholds between 54 and 700 μg/kg. The discriminant analyses performed (linear, quadratic and Mahalanobis) reached classifications above 98% of precision.

The legal limit for the sum of AFB1 in maize subjected to physical treatments before human consumption is 10 μg/kg (European

Table 2
Single-kernel hyperspectral imaging studies for the classification of mycotoxin levels in cereals.

Cereal	Mycotoxin	Type of infection	Spectral range N° of LV used	Preprocessing technique	Reference method	Training/test set Total kernels	Threshold	Classification model (accuracy %)	Reference
Wheat	DON	Natural infection	528-1785 nm 2 LV	–	ELISA	~1320/ ~8720 10,862 total kernels	0.5 mg/kg 1.25 mg/kg	3 classes CM (72%) 2 classes CM (81%)	(Barbedo, Tibola, & Lima, 2017)
		Inoculated	400–2500 nm (Whole range)	–	HPLC-MS	No calibrations performed	–	Spectral signature (R > 0.8)	(Alisaac et al., 2019)
		Natural infection	900–1700 nm (Whole range)	1st Derivative	HPLC	50 total kernels (Cross-validated)	1.25 mg/kg	LDA (98.9%)	(Femenias, Bainotti, et al., 2021)
	OTA	Inoculated	1000-1600 nm 3 LV	–	ELISA	240/60 300 total kernels	78, 120, 400, 580, and 700 µg/kg 54, 91, 220, 402, and 594 µg/kg	Linear, Quadratic and Mahalanobis discriminant analysis (>98%)	(Senthilkumar et al., 2017)
Maize	AFB1	Inoculated 2 LV	400-900 nm	Wavelength subtraction Savitzky-Golay filtering	VICAM AflaTest	243/249 247/245 492 total kernels	20 µg/kg 100 µg/kg	Maximum likelihood (87%) Binary encoding (88%)	(Yao et al., 2010)
		Inoculated 3 LV	1000–2500 nm	Pixel-based mosaic Mask	USDA-FG1S Aflatest	180/30 210 total kernels	10 µg/kg 100 µg/kg	SAM classifier (86.3%)	(Wang et al., 2015a)
		Natural infection 5 LV	1000-2500 nm	Normalization	VICAM AflaTest	80/40 120 total kernels	20 µg/kg 100 µg/kg	SVM (82.5%)	(Chu et al., 2017)
		Mycotoxin spiking 5 LV	1100–2000 nm	Savitzky-Golay smoothing 1st derivative	Kernel spiking	225/225 450 total kernels	10 µg/kg 20 µg/kg 50 µg/kg 100 µg/kg	LDA (88.67%)	(Zhou et al., 2021)
Barley	OTA	Inoculated 3–4 LV	400–2500 nm	–	ELISA	240/60 300 total kernels	140 µg/kg	Linear, Quadratic and Mahalanobis discriminant analysis (100%)	(Senthilkumar et al., 2016)
	DON	Inoculated 3–14 LV	367-1048 nm	CARS-ISSPA	ELISA GC–MS	888/116 1004 total kernels	1.25 mg/kg 3 mg/kg 5 mg/kg 10 mg/kg	PLS-DA 79.2% 90.9% 91.7% 95.8%	(Su et al., 2021)
Oat	DON	Inoculated 6 LV	1000-2500 nm	SNV	GC–MS	31/14 45 total kernels	–	PLS LDA (R 0.8)	(Tekle et al., 2015)
Peanuts	AFB1	Inoculated 3–10 LV	350-2500 nm	Savitzky-Golay algorithm	Artificial contamination	- 146 total kernels	20 µg/kg	RandomForest (89.4%) SVM (62.2%) KNN (88.1%) BP-ANN (80.9%)	(Zhongzhi & Limiao, 2018)

BP-ANN = Backpropagation Artificial Neural Networks; CARS = Competitive adaptive reweighted sampling; CM = Confusion matrix; GA = Genetic algorithm; ISSPA = Iterative selection of successive projections algorithm; KNN = K-Nearest Neighbors; MSC = Multiplicative scatter correction; SAE = Sparse autoencoder; SAM = Spectral angle map.

Commission, 2006b). Thus, the classification of individual kernels according to AFB1 contamination should establish lower sorting thresholds. AFB1 in individual maize kernels were first investigated by two similar studies from the same authors, establishing two limits in 20 and 100 µg/kg (Yao et al., 2010). Although both analyses included the visible spectrum, they used different discrimination tools and reference methods. The results ranged between 84 and 87% and 86–91% for 20 and 100 µg/kg threshold, respectively. On the other hand, other authors worked on the NIR range (1000–2500 nm) with the same purpose. First, Wang et al. (2015b) classified extreme (very high or very low) contaminated kernels with better precision than the 10–100 µg/kg range. Nevertheless, the overall result was 86.3% using the SAM classifier. Then, Chu, Wang, Yoon, Ni, & Heitschmidt (2017) validated a SVM classifier in 3 classes (<20, 20–100, and > 100 µg/kg) with a precision of 82.5%. The study of Zhou, Huang, Liang, & Tian (2021) reported the classification of AFB1 spiked kernels at four different levels (10, 20, 50 and 100 µg/kg). LDA models displayed a 88.67% of accuracy for Savitzky-Golay smoothed and 1st derivate spectra after selecting 5 LV. Despite de high-accuracies, mycotoxin spiking for NIR-HSI analysis does not produce matrix changes in single kernels observed in naturally-infected cereals. In addition, the authors did not analyse the kernels by a reference method, thus the low contaminated kernels could contain already AFB1 from the field or the addition of AFB1 solutions on kernel could increase the levels from the already contaminated kernels. Consequently, the reference levels determined by spiking would not correspond to the real AFB1 concentrations in single kernels. Not in cereals but in almonds, Mishra et al. (2022) quantified AFB1 in single kernels. They obtained optimum PLS models for 2nd derivate spectra

and 7 optimum LV, with an R^2 and RMSEP of 0.96 and 89 μg/kg, respectively.

Different authors analyzed mycotoxins by NIR-HSI (1000–1600 nm) in individual barley kernels. Barley grain sorting according to OTA, which legal limit is 5 mg/kg, was first studied by Senthilkumar et al. (2016). The threshold was 140 mg/kg for different discriminant analyses (linear, quadratic and Mahalanobis). The accuracy reached 100% in the differentiation of OTA contaminated and non-contaminated kernels. Unlike OTA analysis, which was for the NIR region, DON analysis was for Vis-NIR HSI. Complex wavelength selection tools, based on CARS and iterative selection of successive projections algorithm (ISSPA), were used in the study of Su et al. (2021). They established five different thresholds (1.25, 3, 5, and 10 mg/kg), for which the PLS-DA accuracy improved as well as the limit increased (79.2, 90.9, 91.7, and 95.8 %, respectively).

Tekle et al. (2015) investigated DON infection in oat kernels in the NIR region (1000–2500 nm). A positive correlation of 0.8, using a PLS analysis between the spectra from oat and the reference values obtained by GC–MS, was obtained. In addition, they built LDA classification models to identify and visually represent DON infected regions within the wheat kernels. Finally, single peanut kernels were analyzed using similar processes to the used for cereal sorting by HSI (Zhongzhi & Limiao, 2018). AFB1 sorters based on different chemometric and artificial intelligence tools (Random forest, SVM, KNN, BP-ANN) were evaluated by Savitzky-Golay modified spectrum. Models performance were 89.4, 62.2, 88.1, and 80.9%, respectively (threshold of 20 μg/kg). Thus, the results demonstrated the HSI potential to sort single kernels according to mycotoxins levels. However, HSI analysis to discriminate kernels according to mycotoxins seems complex, regarding the low sensitivity of the technique for chemical compounds found naturally in concentrations from mg/kg to low mg/kg or convoluted spectral intensities corresponding to mycotoxins that could be hidden by matrix compounds present in high concentrations. Thus, after several works revision and evaluating the most relevant results, we consider that the discrimination of mycotoxins levels from single kernels relies on the matrix changes in cereal kernels induced by fungal growth. Thus, for the time being, direct mycotoxin measurement with HSI is not feasible, although a broader chemical kernel characterization should be performed, correlating it to the spectral alterations present in mycotoxin contaminated kernels/regions due to the changes produced by fungal metabolism. However, the positive but not high correlation of the fungal and mycotoxin presence can be responsible of misclassifications in single kernel sorting approaches (Paul, Lipps, & Madden, 2005). One of the additional difficulties of single kernel analysis is the characterization of the kernel orientation, as the non-uniformities in kernel shape could cause scattering or dispersions of light. However, controversy exists about the grain orientation effect on the HSI analysis, as some studies reported the feasibility of randomly orientated kernels analysis, while others preferred the one-side analysis (Caporaso, Whitworth, & Fisk, 2017; Delwiche et al., 2019; Shahin & Symons, 2011). Despite the drawbacks of the technique, the classification accuracies could be improved by the scanning of both kernel faces to diminish the orientation effect (Liu et al., 2020). In addition, reference method should measure the mycotoxin levels from single kernels to have the same analytical level of the dependent and independent variables and avoid the already known heterogeneity within a cereal batch. On the other hand, enhanced spectral pretreatments and chemometric techniques also should be applied, extracting information regarding mycotoxin contamination. The studies do not have to focus only on the chemometric results but also on a well-defined and high-quality raw spectra collection, representing the sample features and avoiding light dispersions.

5. Conclusions

The review of the recently published investigations about hyperspectral imaging application to single kernel classification according to fungal and mycotoxin contamination suggests that the heterogeneity management of these contaminants in cereal products is possible. It might be concluded that the results obtained regarding fungal damage discrimination presented positive accuracies that were, in most of the cases, above 90%. On the other hand, the classifications regarding mycotoxin presence showed slightly lower accuracies, the majority between 80 and 100%. Performance differences could be due to the differences in fungal damage produced during its growth, which changes the physicochemical structure of grains, while high mycotoxins levels are present in asymptomatic kernels. Nevertheless, fungal assessment studies predominantly focused on the visual characterization of fungal damages as the reference method. Thus, more precise reference methods are required for future investigations to avoid the introduction of subjectivity. In addition, regarding the laboratory-scale studies reviewed in this article, representative and commonly found field contamination levels are required, obtaining suitable models for routine sorting in the food industry. Concerning mycotoxin contaminations, the threshold established close to the maximum legal limit issued by the food safety authorities, although NIR presents low sensibility near those concentrations. However, the models' performances presented correspond to the management of the differences in majority compound changes due to fungal metabolism associated with mycotoxins production. Thus, the applicability of these techniques as decontamination strategies at post-harvest stages is getting increasingly closer. In conclusion, a first approximation of the potential of HSI as an online sorting strategy before food processing, reducing overall contamination of cereal batches with subsequent health benefits and economic loss reduction, has been demonstrated.

Declaration of Competing Interest

The authors declare that they have no known competing financial interests or personal relationships that could have appeared to influence the work reported in this paper.

Acknowledgements

This work was supported by Project AGL2017-87755-R funded by MCIN/ AEI /10.13039/501100011033/ FEDER "Una manera de hacer Europa" and project PID2020-114836RB-I00 funded by MCIN/ AEI /10.13039/501100011033. The authors are grateful to the University of Lleida (predoctoral grant).

References

Alisaac, E., Behmann, J., Rathgeb, A., Karlovsky, P., Dehne, H. W., & Mahlein, A. K. (2019). Assessment of Fusarium infection and mycotoxin contamination of wheat kernels and flour using hyperspectral imaging. *Toxins, 11*(10), 1–18. https://doi.org/10.3390/toxins11100556

Barbedo, J. G. A., Guarienti, E. M., & Tibola, C. S. (2018). Detection of sprout damage in wheat kernels using NIR hyperspectral imaging. *Biosystems Engineering, 175*, 124–132. https://doi.org/10.1016/j.biosystemseng.2018.09.012

Barbedo, J. G. A., Tibola, C. S., & Fernandes, J. M. C. (2015). Detecting Fusarium head blight in wheat kernels using hyperspectral imaging. *Biosystems Engineering, 131*, 65–76. https://doi.org/10.1016/j.biosystemseng.2015.01.003.

Barbedo, J. G. A., Tibola, C. S., & Lima, M. I. P. (2017). Deoxynivalenol screening in wheat kernels using hyperspectral imaging. *Biosystems Engineering, 155*, 24–32. https://doi.org/10.1016/j.biosystemseng.2016.12.004

Bellon-Maurel, V., & Gorretta, N. (2014). NIR Hyperspectral Imaging for Food and Agricultural Products. In *Infrared and Raman Spectroscopic Imaging* (pp. 295–338). Weinheim, Germany: Wiley-VCH Verlag GmbH & Co. KGaA. https://doi.org/10.1002/9783527678136.ch7.

Boldrini, B., Kessler, W., Rebnera, K., & Kessler, R. W. (2012). Hyperspectral imaging: A review of best practice, performance and pitfalls for in-line and on-line applications. *Journal of Near Infrared Spectroscopy, 20*(5), 483–508. https://doi.org/10.1255/1003

Caporaso, N., Whitworth, M. B., & Fisk, I. D. (2017). Application of calibrations to hyperspectral images of food grains: Example for wheat falling number. *Journal of Spectral Imaging, 6*, 1–15. https://doi.org/10.1255/jsi.2017.a4

Caporaso, N., Whitworth, M. B., & Fisk, I. D. (2018). Near-Infrared spectroscopy and hyperspectral imaging for non-destructive quality assessment of cereal grains.

Applied Spectroscopy Reviews, 53(8), 667–687. https://doi.org/10.1080/05704928.2018.1425214

Chu, X., Wang, W., Ni, X., Li, C., & Li, Y. (2020). Classifying maize kernels naturally infected by fungi using near-infrared hyperspectral imaging. *Infrared Physics & Technology*, *105*(October 2019), 103242. https://doi.org/10.1016/j.infrared.2020.103242.

Chu, X., Wang, W., Yoon, S. C., Ni, X., & Heitschmidt, G. W. (2017). Detection of aflatoxin B1 (AFB1) in individual maize kernels using short wave infrared (SWIR) hyperspectral imaging. *Biosystems Engineering, 157*(17), 13–23. https://doi.org/10.1016/j.biosystemseng.2017.02.005

da Conceição, R. R. P., Simeone, M. L. F., Queiroz, V. A. V., de Medeiros, E. P., de Araújo, J. B., Coutinho, W. M., … de Resende Stoianoff, M. A. (2021). Application of near-infrared hyperspectral (NIR) images combined with multivariate image analysis in the differentiation of two mycotoxicogenic Fusarium species associated with maize. *Food Chemistry*, *344*(July 2019), 128615. https://doi.org/10.1016/j.foodchem.2020.128615.

Del Fiore, A., Reverberi, M., Ricelli, A., Pinzari, F., Serranti, S., Fabbri, A. A., … Fanelli, C. (2010). Early detection of toxigenic fungi on maize by hyperspectral imaging analysis. *International Journal of Food Microbiology, 144*(1), 64–71. https://doi.org/10.1016/j.ijfoodmicro.2010.08.001

Delwiche, S. R., & Kim, M. S. (2000). Hyperspectral imaging for detection of scab in wheat. *Biological Quality and Precision Agriculture II, 4203*, 13–20. https://doi.org/10.1117/12.411752

Delwiche, S. R., Kim, M. S., & Dong, Y. (2010). Damage and quality assessment in wheat by NIR hyperspectral imaging. In M. S. Kim, S.-I. Tu, & K. Chao (Eds.), *Sensing for Agriculture and Food Quality and Safety II* (Vol. 7676, pp. 1–8). https://doi.org/10.1117/12.851150.

Delwiche, S. R., Kim, M. S., & Dong, Y. (2011). Fusarium damage assessment in wheat kernels by Vis/NIR hyperspectral imaging. *Sensing and Instrumentation for Food Quality and Safety, 5*(2), 63–71. https://doi.org/10.1007/s11694-011-9112-x

Delwiche, S. R., Rodriguez, I. T., Rausch, S. R., & Graybosch, R. A. (2019). Estimating percentages of Fusarium-damaged kernels in hard wheat by near-infrared hyperspectral imaging. *Journal of Cereal Science, 87*, 18–24. https://doi.org/10.1016/j.jcs.2019.02.008

Dowell, F. E., Ram, M. S., & Seitz, L. M. (1999). Predicting scab, vomitoxin, and ergosterol in single wheat kernels using near-infrared spectroscopy. *Cereal Chemistry, 76*(4), 573–576. https://doi.org/10.1094/CCHEM.1999.76.4.573

ElMasry, G., & Sun, D.-W. (2010). Principles of Hyperspectral Imaging Technology. In *Hyperspectral Imaging for Food Quality Analysis and Control* (pp. 3–43). Elsevier. https://doi.org/10.1016/B978-0-12-374753-2.10001-2.

European Commission. (2006a). Commission Regulation (EC) N° 1881/2006 of 19 December 2006. Setting maximum levels for certain contaminants in foodstuffs. *Official Journal of the European Communities*, *364*(1881), 5–24.

European Commission. (2006b). Commission regulation (EC) N° 401/2006 of 23 February 2006. Laying down the methods of sampling and analysis for the official control of the levels of mycotoxins in foodstuffs. *Official Journal of the European Union*, *70*(401), 12–34.

Femenias, A., Bainotti, M. B., Gatius, F., Ramos, A. J., & Marín, S. (2021). Standardization of near infrared hyperspectral imaging for wheat single kernel sorting according to deoxynivalenol level. *Food Research International*, *139* (November 2020), 109925. https://doi.org/10.1016/j.foodres.2020.109925.

Femenias, A., Gatius, F., Ramos, A. J., Sanchis, V., & Marín, S. (2021). Near-infrared hyperspectral imaging for deoxynivalenol and ergosterol estimation in wheat samples. *Food Chemistry*, *341*(September 2020), 128206. https://doi.org/10.1016/j.foodchem.2020.128206.

Fox, G., & Manley, M. (2014). Applications of single kernel conventional and hyperspectral imaging near infrared spectroscopy in cereals. *Journal of the Science of Food and Agriculture, 94*(2), 174–179. https://doi.org/10.1002/jsfa.6367

Ito, Y., Srinivasan, C., & Izumi, H. (2006). Discriminant Analysis by a Neural Network with Mahalanobis Distance. In. *Lecture Notes in Computer Science, 3457*, 350–360. https://doi.org/10.1007/11840930_36

Jarvis, J., Haertelt, M., Hugger, S., Butschek, L., Fuchs, F., Ostendorf, R., … Beyerer, J. (2017). Hyperspectral data acquisition and analysis in imaging and real-Time active MIR backscattering spectroscopy. *Advanced Optical Technologies, 6*(2), 85–93. https://doi.org/10.1515/aot-2016-0068

Jiang, L., Zhu, B., & Tao, Y. (2010). Hyperspectral Image Classification Methods. In *Hyperspectral Imaging for Food Quality Analysis and Control (First Edit* (pp. 79–98). Elsevier. https://doi.org/10.1016/B978-0-12-374753-2.10003-6.

Kandpal, L. M., Lee, J., Bae, H., Kim, M. S., Baek, I., & Cho, B. K. (2020). Near-infrared transmittance spectral imaging for nondestructive measurement of internal disorder in Korean Ginseng. *Sensors (Switzerland), 20*(1). https://doi.org/10.3390/s20010273

Karuppiah, K., Senthilkumar, T., Jayas, D. S., & White, N. D. G. (2016). Detection of fungal infection in five different pulses using near-infrared hyperspectral imaging. *Journal of Stored Products Research, 65*, 13–18. https://doi.org/10.1016/j.jspr.2015.11.005

Kos, G., Sieger, M., McMullin, D., Zahradnik, C., Sulyok, M., Öner, T., … Krska, R. (2016). A novel chemometric classification for FTIR spectra of mycotoxin-contaminated maize and peanuts at regulatory limits. *Food Additives and Contaminants - Part A Chemistry, Analysis, Control, Exposure and Risk Assessment, 33* (10), 1596–1607. https://doi.org/10.1080/19440049.2016.1217567

Lee, L. C., Liong, C. Y., & Jemain, A. A. (2018). Partial least squares-discriminant analysis (PLS-DA) for classification of high-dimensional (HD) data: A review of contemporary practice strategies and knowledge gaps. *Analyst, 143*(15), 3526–3539. https://doi.org/10.1039/c8an00599k

Liang, K., Huang, J., He, R., Wang, Q., Chai, Y., & Shen, M. (2020). Comparison of Vis-NIR and SWIR hyperspectral imaging for the non-destructive detection of DON levels in Fusarium head blight wheat kernels and wheat flour. *Infrared Physics & Technology, 106*, Article 103281. https://doi.org/10.1016/j.infrared.2020.103281

Liu, C., Huang, W., Yang, G., Wang, Q., Li, J., & Chen, L. (2020). Determination of starch content in single kernel using near-infrared hyperspectral images from two sides of corn seeds. *Infrared Physics and Technology, 110*(June), Article 103462. https://doi.org/10.1016/j.infrared.2020.103462

Long, Y., Huang, W., Wang, Q., Fan, S., & Tian, X. (2022). Integration of textural and spectral features of Raman hyperspectral imaging for quantitative determination of a single maize kernel mildew coupled with chemometrics. *Food Chemistry*, *372*(August 2021), 131246. https://doi.org/10.1016/j.foodchem.2021.131246.

Lu, B., Sun, J., Yang, N., Wu, X., Zhou, X., & Shen, J. (2018). Quantitative detection of moisture content in rice seeds based on hyperspectral technique. *Journal of Food Process Engineering, 41*(8), 1–7. https://doi.org/10.1111/jfpe.12916

Lu, Y., Huang, Y., & Lu, R. (2017). Innovative hyperspectral imaging-based techniques for quality evaluation of fruits and vegetables: A review. *Applied Sciences (Switzerland), 7*(2). https://doi.org/10.3390/app7020189

Lu, Y., Saeys, W., Kim, M., Peng, Y., & Lu, R. (2020). Hyperspectral imaging technology for quality and safety evaluation of horticultural products: A review and celebration of the past 20-year progress. *Postharvest Biology and Technology, 170*(August), Article 111318. https://doi.org/10.1016/j.postharvbio.2020.111318

M. S. Kim, Y. R. Chen, P. M. M. (1998). Hyperspectral reflectance and fluorescence imaging system for food quality and safety. *Reviews in Economic Geology*, *10*(3), 721–729.

Mahesh, S., Jayas, D. S., Paliwal, J., & White, N. D. G. (2015). Hyperspectral imaging to classify and monitor quality of agricultural materials. *Journal of Stored Products Research, 61*, 17–26. https://doi.org/10.1016/j.jspr.2015.01.006

Manley, M. (2014). Near-infrared spectroscopy and hyperspectral imaging: Non-destructive analysis of biological materials. *Chemical Society Reviews, 43*(24), 8200–8214. https://doi.org/10.1039/c4cs00062e

Mishra, G., Panda, B. K., Ramirez, W. A., Jung, H., Singh, C. B., Lee, S. H., & Lee, I. (2022). Application of SWIR hyperspectral imaging coupled with chemometrics for rapid and non-destructive prediction of Aflatoxin B1 in single kernel almonds. *Lwt*, *155*(December 2021), 112954. https://doi.org/10.1016/j.lwt.2021.112954.

Novakovic, J., & Rankov, S. (2011). Classification performance using principal component analysis and different value of the ratio R. *International Journal of Computers, Communications and Control, 6*(2), 317–327. https://doi.org/10.15837/ijccc.2011.2.2180.

Pasquini, C. (2003). Near infrared spectroscopy: Fundamentals, practical aspects and analytical applications. *Journal of the Brazilian Chemical Society, 14*(2), 198–219. https://doi.org/10.1590/S0103-50532003000200006

Paul, P. A., Lipps, P. E., & Madden, L. V. (2005). Relationship between visual estimates of Fusarium head blight intensity and deoxynivalenol accumulation in harvested wheat grain: A meta-analysis. *Phytopathology, 95*(10), 1225–1236. https://doi.org/10.1094/PHYTO-95-1225

Peiris, K. H. S., Pumphrey, M. O., & Dowell, F. E. (2009). NIR Absorbance characteristics of deoxynivalenol and of sound and Fusarium-damaged wheat kernels. *Journal of Near Infrared Spectroscopy, 17*(4), 213–221. https://doi.org/10.1255/jnirs.846

Polder, G., van der Heijden, G. W. A. M., Waalwijk, C., & Young, I. T. (2005). Detection of Fusarium in single wheat kernels using spectral imaging. *Seed Science and Technology, 33*(3), 655–668. https://doi.org/10.15258/sst.2005.33.3.13.

Qi, X., Jiang, J., Cui, X., & Yuan, D. (2019). Identification of fungi-contaminated peanuts using hyperspectral imaging technology and joint sparse representation model. *Journal of Food Science and Technology, 56*(7), 3195–3204. https://doi.org/10.1007/s13197-019-03745-2

Qin, J. (2010). Hyperspectral Imaging Instruments. In *Hyperspectral Imaging for Food Quality Analysis and Control* (First Edit, pp. 129–172). Elsevier. https://doi.org/10.1016/B978-0-12-374753-2.10005-X.

Qin, J., Kim, M. S., Chao, K., Chan, D. E., Delwiche, S. R., & Cho, B. K. (2017). January 26). *Line-scan hyperspectral imaging techniques for food safety and quality applications. Applied Sciences (Switzerland)*.. https://doi.org/10.3390/app7020125

Ropelewska, E., & Zapotoczny, P. (2018). Classification of Fusarium-infected and healthy wheat kernels based on features from hyperspectral images and flatbed scanner images: A comparative analysis. *European Food Research and Technology, 244*(8), 1453–1462. https://doi.org/10.1007/s00217-018-3059-7

Sahu, J. (2014). Advances in Food Process Engineering. *Introduction to Advanced Food Process Engineering*. https://doi.org/10.1201/b16696-2

Schaare, P. N., & Fraser, D. G. (2000). Comparison of reflectance, interactance and transmission modes of visible-near infrared spectroscopy for measuring internal properties of kiwifruit (Actinidia chinensis). *Postharvest Biology and Technology, 20* (2), 175–184. https://doi.org/10.1016/S0925-5214(00)00130-7

Senthilkumar, T., Jayas, D. S., White, N. D. G., Fields, P. G., & Gräfenhan, T. (2017). Detection of ochratoxin A contamination in stored wheat using near-infrared hyperspectral imaging. *Infrared Physics and Technology, 81*, 228–235. https://doi.org/10.1016/j.infrared.2017.01.015

Senthilkumar, T., Jayas, D. S., White, N. D. G., Fields, P. G., & Gräfenhan, T. (2016). Detection of fungal infection and Ochratoxin A contamination in stored barley using near-infrared hyperspectral imaging. *Biosystems Engineering, 147*, 162–173. https://doi.org/10.1016/j.biosystemseng.2016.03.010

Serranti, S., Cesare, D., & Bonifazi, G. (2012). Hyperspectral-imaging-based techniques applied to wheat kernels characterization. In *Sensing for Agriculture and Food Quality and Safety IV* (Vol. 8369, pp. 83690T-83690T – 13). https://doi.org/10.1117/12.918559.

Shahin, M. A., & Symons, S. J. (2011). Detection of Fusarium damaged kernels in Canada Western Red Spring wheat using visible/near-infrared hyperspectral imaging and

principal component analysis. *Computers and Electronics in Agriculture, 75*(1), 107–112. https://doi.org/10.1016/j.compag.2010.10.004

Shahin, M. A., & Symons, S. J. (2012). Detection of Fusarium damage in Canadian wheat using visible/near-infrared hyperspectral imaging. *Journal of Food Measurement & Characterization, 6*(1–4), 3–11. https://doi.org/10.1007/s11694-012-9126-z

Singh, C. B., Jayas, D. S., Paliwal, J., & White, N. D. G. (2012). Fungal damage detection in wheat using short-wave near-infrared hyperspectral and digital colour imaging. *International Journal of Food Properties, 15*(1), 11–24. https://doi.org/10.1080/10942911003687223

Siripatrawan, U., & Makino, Y. (2015). Monitoring fungal growth on brown rice grains using rapid and non-destructive hyperspectral imaging. *International Journal of Food Microbiology, 199*, 93–100. https://doi.org/10.1016/j.ijfoodmicro.2015.01.001

Su, W.-H., Yang, C., Dong, Y., Johnson, R., Page, R., Szinyei, T., … Steffenson, B. J. (2021). Hyperspectral imaging and improved feature variable selection for automated determination of deoxynivalenol in various genetic lines of barley kernels for resistance screening. *Food Chemistry*, *343*(June 2020), 128507. https://doi.org/10.1016/j.foodchem.2020.128507.

Tekle, S., Mage, I., Segtnan, V. H., & Bjornstad, A. (2015). Near-infrared hyperspectral imaging of Fusarium-damaged oats (Avena sativa L.). *Cereal Chemistry, 92*(1), 73–80. https://doi.org/10.1094/CCHEM-04-14-0074-R

Walsh, K. B., Blasco, J., Zude-Sasse, M., & Sun, X. (2020). Visible-NIR 'point' spectroscopy in postharvest fruit and vegetable assessment: The science behind three decades of commercial use. *Postharvest Biology and Technology, 168*(May), Article 111246. https://doi.org/10.1016/j.postharvbio.2020.111246

Williams, P. J., Geladi, P., Britz, T. J., & Manley, M. (2012). Investigation of fungal development in maize kernels using NIR hyperspectral imaging and multivariate data analysis. *Journal of Cereal Science, 55*(3), 272–278. https://doi.org/10.1016/j.jcs.2011.12.003

Wang, W., Lawrence, K. C., Ni, X., Yoon, S., Heitschmidt, G. W., & Feldner, P. (2015b). *Near-infrared hyperspectral imaging for detecting A fl atoxin B 1 of maize kernels, 51*, 347–355. https://doi.org/10.1016/j.foodcont.2014.11.047

Wang, W., Ni, X., Lawrence, K. C., Yoon, S. C., Heitschmidt, G. W., & Feldner, P. (2015a). Feasibility of detecting Aflatoxin B1 in single maize kernels using hyperspectral imaging. *Journal of Food Engineering, 166*, 182–192. https://doi.org/10.1016/j.jfoodeng.2015.06.009

Williams, P., Manley, M., Fox, G., & Geladi, P. (2010). Indirect Detection of Fusarium verticillioides in Maize (Zea mays L.) Kernels by near Infrared Hyperspectral Imaging. *Journal of Near Infrared Spectroscopy, 18*(1), 49–58. https://doi.org/10.1255/jnirs.858

Wu, N., Jiang, H., Bao, Y., Zhang, C., Zhang, J., Song, W., … Liu, F. (2020). Practicability investigation of using near-infrared hyperspectral imaging to detect rice kernels infected with rice false smut in different conditions. *Sensors and Actuators, B: Chemical*, *308*(June 2019). https://doi.org/10.1016/j.snb.2020.127696.

Yao, H., Hruska, Z., Kincaid, R., Brown, R., Cleveland, T., & Bhatnagar, D. (2010). Correlation and classification of single kernel fluorescence hyperspectral data with aflatoxin concentration in corn kernels inoculated with Aspergillus flavus spores. *Food Additives and Contaminants - Part A Chemistry, Analysis, Control, Exposure and Risk Assessment, 27*(5), 701–709. https://doi.org/10.1080/19440040903527368

Yao, H., Hruska, Z., Kincaid, R., Brown, R. L., Bhatnagar, D., & Cleveland, T. E. (2013). Detecting maize inoculated with toxigenic and atoxigenic fungal strains with fluorescence hyperspectral imagery. *Biosystems Engineering, 115*(2), 125–135. https://doi.org/10.1016/j.biosystemseng.2013.03.006

Yao, H., & Lewis, D. (2010). Spectral Preprocessing and Calibration Techniques. In *Hyperspectral Imaging for Food Quality Analysis and Control* (pp. 45–78). Elsevier. https://doi.org/10.1016/B978-0-12-374753-2.10002-4.

Zhang, H., Paliwal, J., Jayas, D. S., & White, N. D. G. (2007). Classification of Fungal Infected Wheat Kernels Using Near-Infrared Reflectance Hyperspectral Imaging and Support Vector Machine. *Transactions of the ASABE, 50*(5), 1779–1785. https://doi.org/10.13031/2013.23935.

Zhang, M., Li, C., Takeda, F., & Yang, F. (2017). Detection of Internally Bruised Blueberries Using Hyperspectral Transmittance Imaging. *Transactions of the ASABE, 60*(5), 1489–1502. https://doi.org/10.13031/trans.12197.

Zhongzhi, H., & Limiao, D. (2018). Application driven key wavelengths mining method for aflatoxin detection using hyperspectral data. *Computers and Electronics in Agriculture*, *153*(October 2017), 248–255. https://doi.org/10.1016/j.compag.2018.08.018.

Zhou, Q., Huang, W., Liang, D., & Tian, X. (2021). Classification of aflatoxin b1 concentration of single maize kernel based on near-infrared hyperspectral imaging and feature selection. *Sensors, 21*(13), 1–16. https://doi.org/10.3390/s21134257